

Crystallographic phase coexistence, spin-orbital order transitions, and spontaneous spin flop in TmVO_3

C. Ritter,¹ S. A. Ivanov,² G. V. Bazuev,³ and F. Fauth⁴¹*Institut Laue Langevin, 71 avenue des Martyrs, F-38042 Grenoble Cedex 9, France*²*Department of Engineering Sciences, Uppsala University, Box 534, SE-75121 Uppsala, Sweden*³*Institute of Solid State Chemistry, Ural Branch of the Russian Academy of Science, 620999, Ekaterinburg, GSP-145, Russia*⁴*CELLS ALBA Synchrotron, E-08290 Barcelona, Spain*

(Received 6 October 2015; revised manuscript received 1 February 2016; published 24 February 2016)

The thermal evolution of structural and magnetic details of the orthovanadate TmVO_3 , studied in detail by neutron and synchrotron powder diffraction, is reported. Crystallizing in space group $Pnma$ at room temperature, TmVO_3 undergoes a first structural phase transition to $P2_1/a$ at $T_{OO} = 180$ K, where a G -type orbital ordered state develops. At $T_S = 75$ K, a change back to $Pnma$ occurs, and the establishment of C -type orbital order takes place. The V^{3+} ions order antiferromagnetically with a magnetic propagation vector $\mathbf{k} = 0$ below $T_{N1} = 105$ K, while the Tm^{3+} sublattice orders at $T_{N2} = 20$ K following the same propagation vector. Between T_{N1} and T_S , a coexistence of G -type ($P2_1/a$) and C -type ($Pnma$) orbital ordered states exists. The $P2_1/a$ phase is magnetically separated into two fractions, which adopt a $C_x C_y 0$ and $G_x 00$ coupling, respectively, while the $Pnma$ volume fraction follows a $0G_y 0$ magnetic structure. At T_{N2} , the appearance of the Tm sublattice magnetization ($0C_y 0$) leads to a spin flop transition of the V sublattice from $0G_y 0$ to $G_x 00$. The results are presented and analyzed in the general context of the series of $R\text{VO}_3$ compounds, and they are used to discuss recent magnetization results.

DOI: [10.1103/PhysRevB.93.054423](https://doi.org/10.1103/PhysRevB.93.054423)

I. INTRODUCTION

Transition metal perovskites of type $R\text{TO}_3$ (where R is a rare earth or Y) have attracted enormous interest in condensed matter physics over the last 25 years due to the plethora of interesting electronic and magnetic properties they show. While manganites became famous for the existence of charge and orbital ordering phenomena and for related giant magnetoresistance and ferroelectric properties [1–3], cobaltates were intensively studied for the occurrence of spin state transitions and nonconventional metal-insulator transitions [4–6]. The appearance of an unusual magnetic order and of charge disproportionation in combination with a sharp metal-insulator transition was discussed in nickelates [7–9]. Vanadates were less studied until anomalous diamagnetism for LaVO_3 [10] and a temperature induced multiple magnetization reversal was found for YVO_3 [11], which triggered numerous studies on the crystallographic, magnetic, and electronic properties of the $R\text{VO}_3$ family of compounds.

All $R\text{VO}_3$ compounds adopt at room temperature a distorted perovskite structure with space group $Pnma$ with one single Wyckoff site $4b$ for the V cation [12]. The lattice parameters are linked to the original undistorted cubic perovskite structure by $a \approx c \approx \sqrt{2}a_p$ and $b \approx 2a_p$, where a_p corresponds to the lattice parameter of the cubic phase. Specific heat data [13] showed two phase transitions for YVO_3 : a second-order transition at $T_N = 115$ K, reflecting the appearance of long-range magnetic order, and a first-order structural transition at $T_S = 78$ K, where a change of the magnetic structure takes place simultaneously [14]. The structural transition is accompanied by changes of the lattice parameters, which lead to an anisotropy in the V-O bonds within the VO_6 octahedra, and this was linked to the creation of a G -type orbital order. Kawano *et al.* [15] reinvestigated the magnetic structures of YVO_3 and found a change from C -type antiferromagnetic (AFM) to G -type AFM at T_S . Their results opened the way as

well for a better understanding of the crystallographic structure for $T > T_S$. Postulating that the change of the magnetic structure from G -type below T_S to C -type above T_S has to be accompanied by a change of the orbital order as well, Ren *et al.* [16] deduced that G -type orbital order (OO) has to be present above T_S . The appellations “ C -type” and “ G -type” follow here the classification of magnetic structures in these perovskites. Both types of orbital order denote an alternate occupation of the $d_{xy}d_{yz}$ and $d_{xy}d_{xz}$ orbitals between adjacent V sites within the ac plane. If this alternate order expands along the b direction, the G -type OO is formed, whereas the C -type OO is created through the superposition of identical orbitals on adjacent V sites in the b direction [17–19]. Because the formation of G -type orbital order is not possible in the orthorhombic $Pnma$ space group—indeed this symmetry does not allow the presence of differently distorted ac planes—the crystal structure above T_S has to be of lower symmetry. Neutron diffraction and synchrotron x-ray diffraction revealed that YVO_3 adopts most probably the monoclinic space group $P2_1/a$ above T_S and stays in this orbital ordered phase even above T_N , until a second structural transition takes place at $T_{OO} \approx 200$ K [19]. The same monoclinic space group had already been proposed before by Bordet *et al.* [20] for LaVO_3 below 140 K, where this compound, which is formed with the R cation having the largest ionic radius, displays a nearly coupled crystallographic-magnetic transition. The transition to the OO state at T_{OO} leads to relatively small changes in the structural parameters and is therefore less visible than, for example, in the manganites. This is due to the fact that the Jahn-Teller interactions are weaker in the orthovanadates as only the t_{2g} orbital electrons are active. An even further reduction of the symmetry through dimerization in the b direction and formation of singlet orbital spin-Peierls states was proposed to occur in YVO_3 [21] and was discussed as a possible reason for the reduced ordered magnetic moment of the G -type orbital ordered phase [22].

Miyasaka *et al.* [23] proposed a first phase diagram of the RVO_3 system as function of the ionic radius of the R cation. A clear division was made between compounds with small ionic radii, $R = \text{Lu-Dy}$, and those with larger R ions (Tb-La). While the former exhibit structural transitions at T_{OO} , where the monoclinic structure with G -type orbital order sets in, and at T_S , where the orbital order changes to C -type and the structure changes back to orthorhombic, and a magnetic transition at T_N , with a sequence $T_{OO} > T_N > T_S$, the latter see only T_{OO} and T_N and stay therefore down to lowest temperatures in a G -type orbital ordered state. An exception to this sequence was said to exist for CeVO_3 , where $T_N > T_{OO}$ was claimed and included in the phase diagram. This apparent inconsistency was, however, solved by Reehuis *et al.* [24], who showed that here as well, $T_{OO} > T_N$, as expected. Previously, Reehuis *et al.* [25] had proposed that above T_S within the G -type orbitally ordered phase, YVO_3 still shows short-range C -type orbital order and a magnetic structure of type $C_x G_y C_z$, which is not allowed from magnetic symmetry analysis [26]. A phase separation scenario with the coexistence of the low temperature orthorhombic phase and the monoclinic phase was explicitly excluded. The trend of the magnetic ordering transition at T_N to decrease in temperature with decreasing ionic radius was connected to the increasing octahedral distortion, which leads to a stronger localization of the $3d$ electrons and a weakening of the V-O-V superexchange interactions [27]. The opposing influences of the octahedral distortion and of the magnetic exchange striction on the appearance of the different orbitally ordered states as a function of the R ionic radius were discussed in detail by Sage *et al.* [28]. The phase diagram was modified substantially by adding a region of phase coexistence of orthorhombic $Pnma$ and monoclinic $P2_1/a$ phases for $R = \text{Tb-Nd}$, which opens up slightly below T_N . This phase coexistence goes in line with a coexistence of orbital ordered C -type and G -type phases and excludes therefore a sharp phase boundary between the two states as a function of the ionic radius of R^{3+} . For SmVO_3 , it was found that the monoclinic angle of the G -type orbitally ordered phase increases strongly as the C -type OO phase, which has a lower volume, sets in [29]. Interestingly enough, Reehuis *et al.* [25] did not find any sign of this phase coexistence in their single-crystal studies on TbVO_3 and NdVO_3 . These findings point towards a strong influence of internal strain on the microscopic behavior of the system and to a possible difference between powder and single-crystal samples.

Although knowledge of the magnetic and structural behavior of the rare earth orthovanadates RVO_3 has enormously increased over the last 20 years, several questions remain to be solved, especially for the part of the phase diagram where $r_R^{3+} \leq r_{\text{Dy}}^{3+}$. The rare studies that exist are limited to only partial aspects of the general problem. Munoz *et al.* [30] refined a G -type magnetic structure for YbVO_3 at 2 K assuming a monoclinic structure but did not reflect on the existence of a possible reentrant structural transition to an orthorhombic structure as expected for this part of the phase diagram. For $R = \text{Er, Ho, and Dy}$, Reehuis *et al.* [31] determined the different magnetic structures as function of temperature from single-crystal neutron diffraction but did not perform any detailed low temperature crystal structure studies. The existence of the sequence $T_{OO} > T_N > T_S$ was deduced for

HoVO_3 from the temperature dependence of some nuclear reflections and for ErVO_3 and DyVO_3 in analogy to YVO_3 from the temperature dependence of the magnetic structures. The magnetic structure of the V sublattice within the monoclinic phase region was determined to be $C_x G_y C_z$ ($P2_1/a$ or $Pnma$ setting) for $R = \text{Dy, Ho, and Er}$, similar to YVO_3 , and therefore again not compatible with magnetic symmetry analysis. There exists no determination of the structural details of the monoclinic phase in this phase region apart from that on YVO_3 . As the temperature-induced change from G -type orbital order to C -type orbital order in YVO_3 was connected to a slight increase in the octahedral distortion as the temperature was lowered, and the characteristics of G -type and C -type OO are best seen in the individual V-O bond lengths and V-O-V bond angles, a systematic temperature-dependent study of a further RVO_3 compound with $r_R^{3+} \leq r_{\text{Dy}}^{3+}$ is clearly required.

In a recent study, some of us determined the existence of successive phase transitions in TmVO_3 from magnetization and specific heat measurements [32]. Four transition temperatures were linked to the onset of orbital order at $T_{OO} = 175$ K, the appearance of magnetic order at $T_{N1} = 108$ K, a spin-orbital transition at $T_S = 78$ K, and to the magnetic order of the Tm sublattice at $T_{N2} = 15$ K. The presence of the transitions $T_{OO} > T_N > T_S$ and of a magnetization reversal at T_S resembles strongly the situation in YVO_3 . The ionic radius of Tm^{3+} situates TmVO_3 between YbVO_3 and ErVO_3 and therefore in the part of the phase diagram of RVO_3 compounds where more structural studies are needed to allow a comparison to the situation in YVO_3 .

This paper presents detailed results of a temperature dependent diffraction study using high intensity and high angular resolution neutron powder diffraction as well as x-ray synchrotron radiation. The evolution of the structural parameters and of the magnetic structures of TmVO_3 is followed and shows that a G -type orbital ordering at T_{OO} leads to strongly differing V-O distances, to a change of space group to $P2_1/a$, and, at T_{N1} , to the formation of a predominantly C -type magnetic order with spin components $C_x C_y$, which are allowed by magnetic symmetry analysis. At T_S , a structural transition back to the $Pnma$ space group with C -type OO is accompanied by a change to the G -type magnetic structure possessing a single component G_y . Clear evidence for phase coexistence of $Pnma$ and $P2_1/a$ in the temperature region around T_S is given. This nuclear phase coexistence goes along with the coexistence of the two associated magnetic structures. The ordering at T_{N2} of the Tm sublattice in a C_y -type magnetic structure leads to a spin flop transition of the vanadium sublattice from G_y to G_x . These results will be discussed in comparison with published data on other RVO_3 compounds.

II. EXPERIMENTAL DETAILS

The preparation and magnetic characterization of the powdered sample of TmVO_3 has been described in [32]. Neutron powder diffraction data were taken on the high resolution powder diffractometer D2B and on the high intensity powder diffractometer D20, both situated at the Institut Laue Langevin, Grenoble, France. In total, 17 data points were recorded on D2B with $\lambda = 1.5947 \text{ \AA}$ on heating between 1.5 and 300 K, putting special emphasis on the temperature regions

around T_S and T_N . The instrumental angular resolution of one measurement at 85 K was optimized by using a 10' collimation of the primary neutron beam and by placing additional slits behind the monochromator in order to limit the wavelength spread of the monochromatic beam. Additional data were taken on cooling down at 90 K and 80 K using the optimized resolution. A first thermodiffraction was measured on D20 by ramping up the temperature at a speed of 0.3 K/min between 1.7 K and 240 K and taking spectra every 5 min. A wavelength of $\lambda = 2.4156 \text{ \AA}$ was selected using a Ge (113) monochromator at a takeoff angle of 90° , representing a high resolution option of this instrument [33]. A second thermodiffraction was taken under the same conditions but on cooling down between 120 K and 1.7 K. Several longer (20 min) data points were additionally taken between 60 K and 110 K and between 85 K and 100 K (60 min) in the high flux option of D20 using a highly oriented pyrolytic graphite (HOPG) monochromator at the low takeoff angle of 42° , giving $\lambda = 2.4165 \text{ \AA}$. Synchrotron experiments were performed on

TABLE I. Lattice constants, atomic parameters, and thermal parameters as determined from the refinement of the neutron data in $Pnma$ (300 K, 50 K) and $P2_1/a$ (120 K). Due to the extremely small scattering length of V, no thermal B factors were refined for this atom type.

T (K)	300	120/110 ^a	50
Space group	$Pnma$	$P2_1/a$	$Pnma$
a (Å)	5.5851(1)	5.5904(1) 5.59172(2) ^a	5.5603(1)
b (Å)	7.5535(1)	7.5222(1) 7.52061(3) ^a	7.5359(1)
c (Å)	5.2461(1)	5.2442(1) 5.24382(2) ^a	5.2526(1)
γ (°)	—	90.010(7) 90.011(1) ^a	—
Tm: x	0.0693(2)	0.0700(3)	0.0703(2)
y	$\frac{1}{4}$	$\frac{1}{4}$ (fixed)	$\frac{1}{4}$
z	0.9798(3)	0.9794(3)	0.9794(3)
U_{iso}	0.0056(3)	0.0033(4)	0.0020(4)
V_1 : x	$\frac{1}{2}$	$\frac{1}{2}$	$\frac{1}{2}$
y	0	0	0
z	0	0	0
V_2 : x	—	0	—
y	—	$\frac{1}{2}$	—
z	—	$\frac{1}{2}$	—
O_1 : x	0.4572(3)	0.4571(3)	0.4581(3)
y	$\frac{1}{4}$	$\frac{1}{4}$ (fixed)	$\frac{1}{4}$
z	0.1152(3)	0.1163(3)	0.1174(3)
U_{iso}	0.0080(4)	0.0062(4)	0.0051(4)
O_2 : x	0.3058(2)	0.3126(10)	0.3008(2)
y	0.0583(1)	0.0580(12)	0.0599(1)
z	0.6899(2)	0.6940(10)	0.6862(2)
U_{iso}	0.0081(3)	0.0052(14)	0.0048(3)
O_3 : x	—	0.7005(9)	—
y	—	0.5601(13)	—
z	—	0.3161(11)	—
U_{iso}	—	0.0049(14)	—
R_{Bragg}	4.3	4.1	4.4

^aFrom high resolution synchrotron powder data.

the powder diffraction station of the BL04-MSPD beamline [34] of the ALBA synchrotron located in the Barcelona area, Spain. Data were collected in transmission mode using the 13 channel multianalyzer detection (MAD) setup—220 Bragg reflection of silicon crystal—which offers the highest possible instrumental angular resolution ($\Delta 2\Theta \sim 0.005^\circ$). In order to minimize absorption, patterns were recorded at short wavelength, $\lambda = 0.31776 \text{ \AA}$, and with the sample filled in a 0.5-mm-diameter borosilicate capillary. Data were registered on cooling at several temperatures between 295 K and 80 K and on heating at 110 K and 150 K. Low temperatures were achieved using a liquid nitrogen cryostream (Oxford Cryosystems Series 700). While the use of the neutron data is due to its comparatively high scattering cross section, which is advantageous for the exact determination of the oxygen positions, the superior resolution of the synchrotron data allows the exact refinement of unit cell parameters. All diffraction data were refined by the Rietveld method using the FullProf [35] refinement package. Magnetic symmetry analysis was done using the program BASIREPS [36,37], included in the FullProf suite.

III. RESULTS AND DISCUSSION

A. Temperature dependence of structural parameters

High resolution data confirm the $Pnma$ crystal structure of TmVO_3 at 300 K and exclude the presence of impurities. Structural details are listed in Table I. Several transitions of structural and/or magnetic origin are visible in the thermodiffraction shown in Fig. 1. The transition situated at about 180 K is in accordance with the knowledge gained from the other $R\text{VO}_3$ compounds tentatively attributed to an orbital ordering transition. Synchrotron data taken below T_{OO} confirm the change to the monoclinic space group $P2_1/a$, which leads to the existence of two independent V sites.

The high resolution neutron data were accordingly refined below T_{OO} in $P2_1/a$ and revealed the occurrence of strongly enhanced differences in the V-O bond distances within the

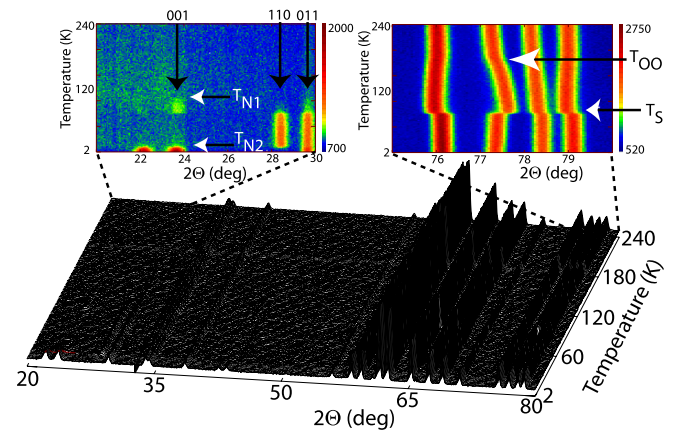


FIG. 1. Neutron thermodiffraction of TmVO_3 between 2 K and 240 K. The left inset shows a contour plot of the low 2Θ angle region with the appearance of magnetic reflections at T_{N1} and T_{N2} ; the right inset displays a high 2Θ angle region, where the structural transitions at T_{OO} and T_S are visible through strong shifts in the position of Bragg reflections.

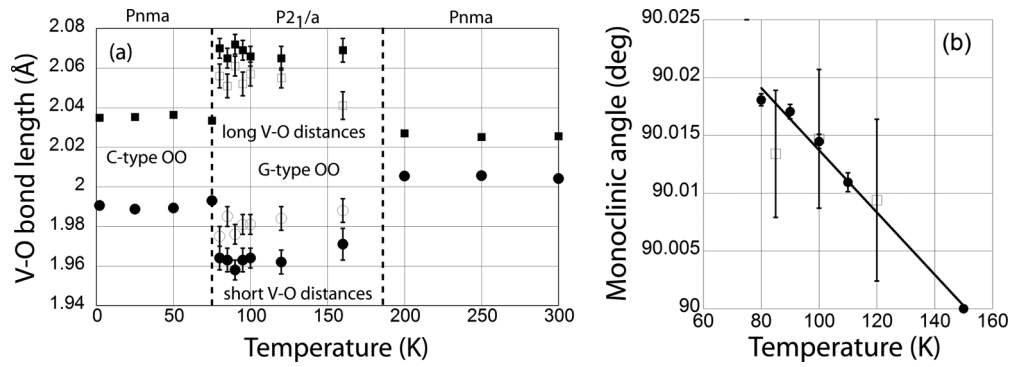


FIG. 2. (a) Variation of the V-O bond lengths with temperature as determined from high resolution neutron data of D2B. Note appearance of *G*-type OO below 180 K and of *C*-type OO below 75 K. (b) Variation of the monoclinic angle with temperature refined from synchrotron (closed circles) and neutron (open squares) data.

ac plane reflecting the orbitally ordered state Fig. 2(a). The distortion from the orthorhombic lattice is very small, with the monoclinic angle increasing linearly from 90° at 150 K to about 90.018 (1°) at 80 K Fig. 2(b).

Table I lists the structural details of the refinement of the neutron data taken at 120 K. Due to the very small value of the monoclinic angle, it was possible to perform a cyclic Le Bail fit of the 143 data sets between 2 K and 240 K in space group *Pnma* in order to determine the thermal variation of the lattice parameters. Hereby, the low angle 2Θ region where magnetic peaks appear at low temperatures were excluded from the refinement. At $T_{OO} \sim 180$ K, changes in the slope of all three lattice parameters are visible Figs. 3(a)–3(c). They, however, compensate for each other and lead to a monotonic behavior of the thermal expansion over T_{OO} Fig. 3(d). A jump of all three lattice parameters leading to a volume contraction is visible at around $T_S = 75$ K and is related to a second structural transition, which indicates the change from the *P2₁/a* phase having *G*-type OO back to a *Pnma* phase with now *C*-type OO. No anomaly is visible at the magnetic transition at $T_{N1} = 105$ K (Fig. 1), where the V sublattice becomes magnetic (see Sec. III B), while small changes in the thermal variation of the lattice parameters are visible at $T_{N2} \approx 20$ K, where the Tm sublattice orders magnetically (see Sec. III C).

The second thermodiffractionogram recorded on cooling down was analyzed in the same way and did not reveal any significant thermal hysteresis when comparing it to the data taken on

heating up. The strong volume contraction is again positioned at $T_S = 75$ K, while small changes in the lattice parameters are seen at around $T_{OO} = 180$ K.

We will now turn to the discussion of the temperature dependence of some structural details. Figure 4(a) displays the behavior of the octahedral tilting represented by the V-O₁-V angle along the long *b* direction: A nearly linear increase of this angle corresponding to a decrease of the tilting can be determined for the temperature region between base temperature and 75 K and between 200 K and 300 K within the *Pnma* phase regions. At T_S , at the transition into the *P2₁/a* phase, the angle jumps to a smaller value before it increases in an accelerated way up to T_{OO} , where the reentrance into the *Pnma* phase region takes place.

Analyzing the data for YVO_3 , Blake *et al.* [19] postulated that the increase of the octahedral tilting drives the system from a *G*-type OO (*P2₁/a*) to a *C*-type OO (*Pnma*). The data on TmVO_3 show now that the situation is more complicated: At T_S , the octahedral tilting becomes larger (the V-O₁-V angle decreases; Fig. 4(a)) when entering the *P2₁/a* phase. The argument of Blake *et al.* still holds, however, if we assume that there is an upper stability limit for the *P2₁/a* phase to support the octahedral tilting. In this context, it is interesting to discuss the thermal contraction of TmVO_3 . Figures 3(a)–3(d) show that below T_{OO} , the thermal contraction is solely determined by the strong decrease of the *b* axis of the *P2₁/a* phase. There are two ways for the structure to accommodate

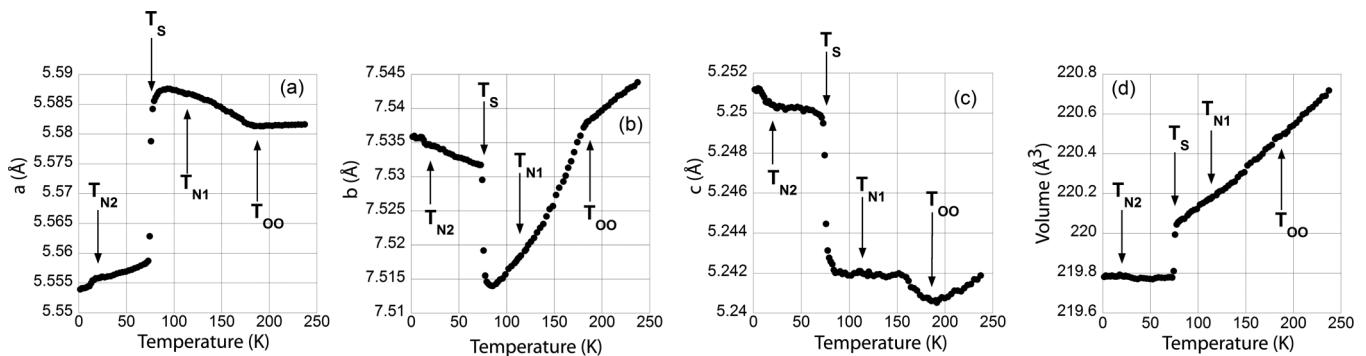


FIG. 3. Thermal variation of the lattice parameters of TmVO_3 (a,b,c) and of the volume (d) as determined from high intensity neutron data using D20 in the 90° takeoff angle, high resolution option.

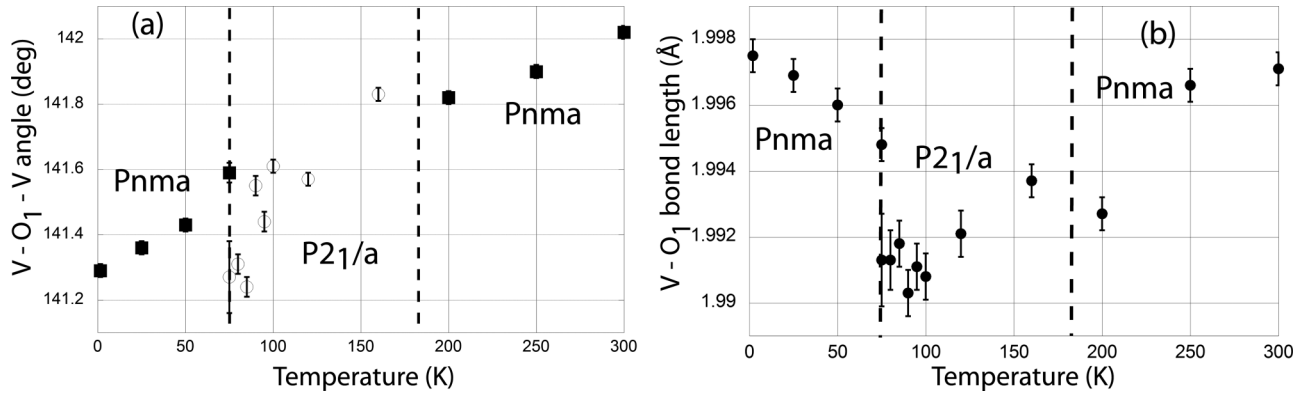


FIG. 4. Variation of the V-O₁-V angle (a) and of the V-O₁ bond length (b) as a function of temperature as determined from high resolution neutron data of D2B.

this contraction: either by a decrease of the V-O₁ distances or by an increase of the octahedral tilting. Figures 4(a) and 4(b) show that both effects take place between T_{OO} and 100 K. Below 100 K, however, the volume contraction is only absorbed by the increase of the tilting, while the V-O₁ distances stay constant. It seems that the V-O₁ distances cannot be compressed more strongly, a fact which could indicate the stability limit of the $P2_1/a$ phase, where the G -type OO can no longer be supported by the structure, and a transition to the C -type OO at T_S sees a relief of both the V-O₁ distances and of the octahedral tilting.

Following an idea by Goodenough [38], Mizokawa *et al.* [39] calculated the stability of the different orbitally ordered states as a function of the octahedral tilting and the induced change in the covalence between the A site and the oxygen ions. They concluded that the increasing octahedral tilting should lead to a shift of the R cation, which favors the C -type OO with respect to the G -type OO for large tilting angles. While within the G -type OO phase, this shift is along the [10 $\bar{1}$] direction ($Pnma$ setting), it changes into the [001] direction within the C -type OO phase, thereby keeping closest contact to the four nearest neighbor oxygen ions. For TmVO₃, this effect can be seen in Fig. 5, where the temperature dependent

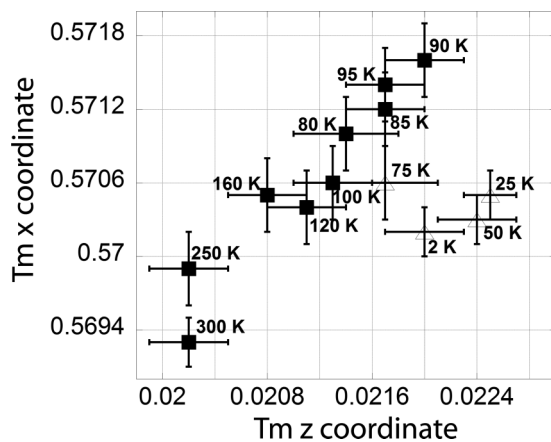


FIG. 5. Variation of the x and z coordinates of Tm with temperature as determined from high resolution neutron data of D2B. Squares represent the high temperature and the G -type OO phases; open triangles represent the C -type ordered OO phase.

displacement of the Tm cation can be related to the increasing octahedral tilting [Fig. 4(a)] and to the change to the C -type OO below 80 K [as will be seen in Fig. 10(a)].

B. Magnetic order of the V sublattice for $T > T_{N2}$ phase coexistences

In the temperature range between T_{N1} and T_S , the magnetic intensities are very low (Fig. 6), and a difference pattern between 85 K and 110 K using the high intensity D20 data is used to visualize the pure magnetic peaks (Fig. 7). They can be indexed with the magnetic propagation vector $\mathbf{k} = 0$. Magnetic symmetry analysis (Table II) shows that for each of the two vanadium sites, there are two allowed irreducible representations (IR), each containing three basis vectors (BV). Assuming that the same IR is acting on the two vanadium sites, and assuming equal moments on both vanadium sites, the two IRs can be—depending on the parallel or antiparallel alignment of the two sites—combined to give four different allowed magnetic structures (Table II). In order to refine the intensities of the six clearly visible magnetic peaks, one has to assume concurrent contributions from C -type and G -type spin order (SO), which is not an allowed solution from magnetic symmetry analysis.

Even when trying to combine BVs from two different IRs (e.g., $G_x G_y C_z$ or $C_x C_y G_z$), it is not possible to calculate the correct intensities. Only when assuming the coexistence of two IRs, both having two nonzero BVs, namely, $C_x C_y 0$ and $G_x G_y 0$, is it possible to refine the data. The persistence of G -type SO above T_S within the G -type OO phase has been mentioned before by Reehuis *et al.* [25] for YVO₃. While Reehuis *et al.* excluded the possibility of a coexistence of two different nuclear phases and assumed a spin-canted state, our high resolution neutron data taken at 85 K prove the coexistence of the $P2_1/a$ and the $Pnma$ nuclear phases. The two phase refinement of the data is shown in Fig. 8; the inset displays a 2Θ range where Bragg peaks characteristic for each phase are well separated. The detection of the phase coexistence (86% $P2_1/a$, 14% $Pnma$) is facilitated by relatively large differences in the lattice parameters (Table I). The same coexistence was found in the 75 K data, with now the majority phase being $Pnma$ (79%). Data taken on cooling show that this phase coexistence is also present in similar

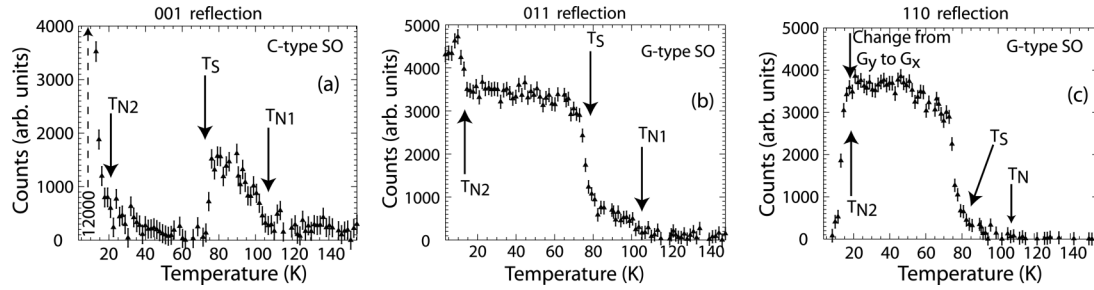


FIG. 6. Variation of the integrated intensity of three characteristic magnetic reflections with temperature: 001 (a), 011 (b), and 110 (c).

proportions when coming from $T > T_N$. This proves that the phase coexistence is not the result of an incomplete phase transition from $Pnma$ to $P2_1/a$ at T_S when coming from low temperatures, but is characteristic for the temperature region between T_S and T_N independent of the thermal history.

This phase coexistence immediately suggests that the magnetic peaks visible in the difference data files are stemming from two different nuclear phases: the C -type SO components from the $P2_1/a$ phase, and the G -type components from the $Pnma$ phase. By fixing the atomic coordinates and the lattice parameters to the values determined in the refinement of the high resolution D2B data taken at 85 K, the corresponding high intensity data taken also at 85 K on D20 were refined in order to determine scale factors for the two nuclear phases. The phase ratio was 85%/15%, i.e., nearly identical to the previously determined value. Using these scale factors, the purely magnetic pattern can be refined, with $C_x C_y 0$ SO ($R_{Mag} = 9.5\%$) within the $P2_1/a$ phase and $G_x G_y 0$ SO ($R_{Mag} = 5.0\%$) within the $Pnma$ phase. The components amount to $C_x = 0.82(1)\mu_B$, $C_y = 0.32(2)\mu_B$, and

$G_x = 1.00(5)\mu_B$, $G_y = 1.19(5)\mu_B$, giving total moments of $0.88(1)\mu_B$ for the $P2_1/a$ phase and $1.56(4)\mu_B$ for the $Pnma$ phase, respectively. There is, however, no IR of type $G_x G_y 0$ in $Pnma$ [26], and the magnetic moment value refined for the $Pnma$ phase of $1.56\mu_B$ is surprisingly high compared to the low temperature value, *vide infra*. The high resolution data taken below T_S at 50 K indicate the unique presence of the $Pnma$ phase at this temperature (Table I) and a C -type OO. The V-O bond lengths within the basal plane of the VO_6 octahedra are now less different than in the G -type OO phase but still significantly more different Fig. 2(a) when compared to the orbitally disordered $Pnma$ phase above T_{OO} . The magnetic structure is of G -type following the allowed IR $C_x G_y F_z$, with $C_x = F_z = 0$ and $G_y = 1.33(3)\mu_B$, with the magnetic moment pointing in the direction of the long b axis. The size of the magnetic moment and the magnetic structure were confirmed using high intensity data, which gave $G_y = 1.28(3)\mu_B$. It is unlikely that the magnetic structure of

TABLE II. BVs of the two IRs of the vanadium atoms V_1 and V_2 located, respectively, on the Wyckoff positions $2c$ and $2d$ for the magnetic propagation vector $\mathbf{k} = 0$ in space group $P2_1/a$. Combination of the BVs of the two V sites by assuming either a ferromagnetic or an antiferromagnetic alignment leads to the allowed couplings $G_x G_y F_z$, $C_x C_y A_z$ (IR1), and F_x , F_y , G_z , A_x , A_y , C_z (IR2).

V_1	IR1			IR2		
	BV1	BV2	BV3	BV1	BV2	BV3
$\frac{1}{2} 0 0$	1 0 0	0 1 0	0 0 1	1 0 0	0 1 0	0 0 1
$0 0 \frac{1}{2}$	-1 0 0	0 -1 0	0 0 1	1 0 0	0 1 0	0 0 -1
			V_2			
$0 \frac{1}{2} \frac{1}{2}$	1 0 0	0 1 0	0 0 1	1 0 0	0 1 0	0 0 1
$\frac{1}{2} \frac{1}{2} 0$	-1 0 0	0 -1 0	0 0 1	1 0 0	0 1 0	0 0 -1
	V_1 ferromagnetically aligned to V_2					
$\frac{1}{2} 0 0$	1 0 0	0 1 0	0 0 1	1 0 0	0 1 0	0 0 1
$0 0 \frac{1}{2}$	-1 0 0	0 -1 0	0 0 1	1 0 0	0 1 0	0 0 -1
$0 \frac{1}{2} \frac{1}{2}$	1 0 0	0 1 0	0 0 1	1 0 0	0 1 0	0 0 1
$\frac{1}{2} \frac{1}{2} 0$	-1 0 0	0 -1 0	0 0 1	1 0 0	0 1 0	0 0 -1
	G_x	G_y	F_z	F_x	F_y	G_z
	V_1 antiferromagnetically aligned to V_2					
$\frac{1}{2} 0 0$	1 0 0	0 1 0	0 0 1	1 0 0	0 1 0	0 0 1
$0 0 \frac{1}{2}$	-1 0 0	0 -1 0	0 0 1	1 0 0	0 1 0	0 0 -1
$0 \frac{1}{2} \frac{1}{2}$	-1 0 0	0 -1 0	0 0 -1	-1 0 0	-0 1 0	0 0 -1
$\frac{1}{2} \frac{1}{2} 0$	1 0 0	0 1 0	0 0 -1	-1 0 0	-0 1 0	0 0 1
	C_x	C_y	A_z	A_x	A_y	C_z

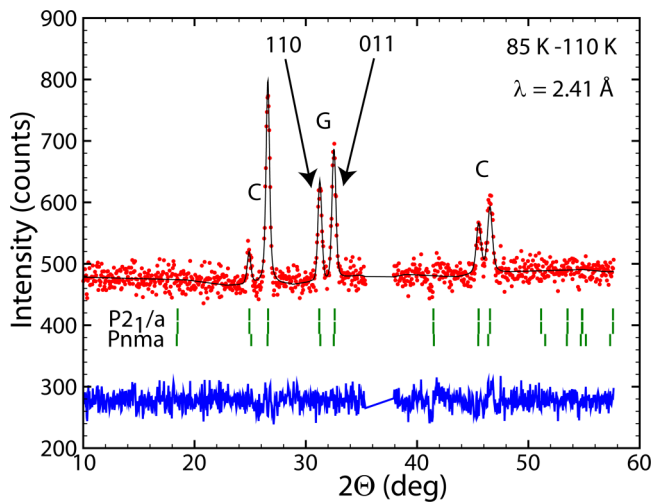


FIG. 7. Rietveld refinement of the difference pattern between 85 K and 110 K of $TmVO_3$ showing purely magnetic scattering of V^{3+} . The dots (red) and the solid line (black) represent the observed and calculated intensities, respectively, and the line below (blue) indicates the difference between them. Tick marks indicate the calculated positions of allowed magnetic Bragg peaks for $P2_1/a$ (upper two rows) and $Pnma$ (lower row). The two magnetic peaks created by the G -type magnetic order have been indexed (see main text).

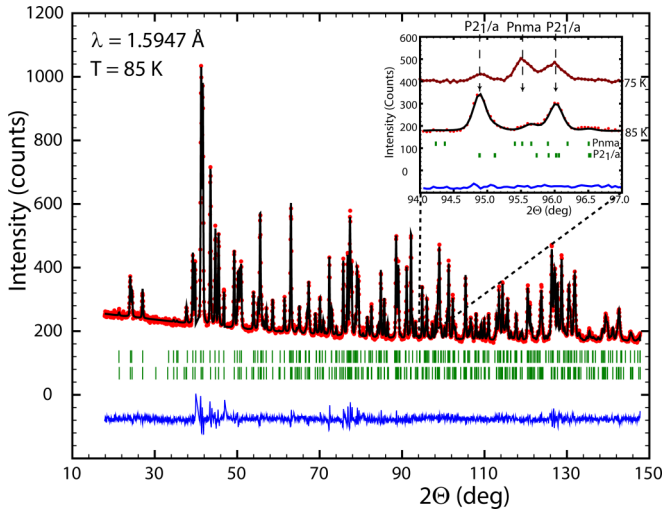


FIG. 8. Observed (red dots), calculated (black line), and difference pattern of the refinement of the nuclear structure only of TmVO_3 at 85 K. The tick marks indicate the calculated positions of the $Pnma$ (upper row) and $P2_1/a$ (lower row) phases.

the low temperature $Pnma$ phase increases the moment size when entering the phase coexistence region on heating, and this raises questions for the above presented solution for the 85 K data. Taking up the proposition of Reehuis *et al.* [25] for YVO_3 , it was therefore assumed that the $P2_1/a$ phase possesses as well a G -type component in its SO. By testing all possible orientations of the C and G components, good refinements were achieved for the $T = 85$ K data using models with either (1) $C_x C_y G_z / G_x 00$ or (2) $C_x G_y C_z / G_x 00$ for the $P2_1/a$ phase and $Pnma$ phase, respectively. The magnetic R factors are significantly lower in these models compared to the $C_x C_y 0$ ($P2_1/a$)/ $G_x G_y 0$ ($Pnma$) model presented above, and the magnetic moment of the $Pnma$ phase is similar for (1) with $1.33(2) \mu_B$ and slightly lower for (2) with $1.15(2) \mu_B$ as at 50 K, where the $Pnma$ phase is the unique phase present. Let us recall here that the $C_x G_y C_z$ SO had been proposed by Reehuis *et al.* [25] for the $P2_1/a$ phase of YVO_3 . There are, however, three arguments that speak against these solutions for the magnetic order in the phase coexistence region. First of all, neither a SO of type $C_x C_y G_z$ nor of type $C_x G_y C_z$ would represent an allowed IR for the $P2_1/a$ phase, and second of all, a $G_x 00$ model for the SO of the $Pnma$ phase at 85 K would mean that the SO of this $Pnma$ phase sees a spin reorientation between $T < T_S$, where the SO is $0G_y 0$ and $T > T_S$ as it becomes the minority phase.

The third argument against these solutions is based on the temperature dependence of the magnetic peaks: The high resolution neutron diffraction data taken on D2B and D20 permit us to quantify the coexistence of the two phases $Pnma$ and $P2_1/a$ on heating in the temperature region $70 \text{ K} < T < 110 \text{ K}$. The phase percentage of the $Pnma$ phase is seen to decrease from about 15% at 85 K down to about 7% at 105 K. At the same time, data taken between 85 K and 100 K with very high statistics (60 min/point) show that all magnetic peaks are present up to T_N , with, however, a change in the intensity ratio between the two magnetic peaks (110, 011) created through G -type SO (Fig. 9). The relative intensities of the 110 and

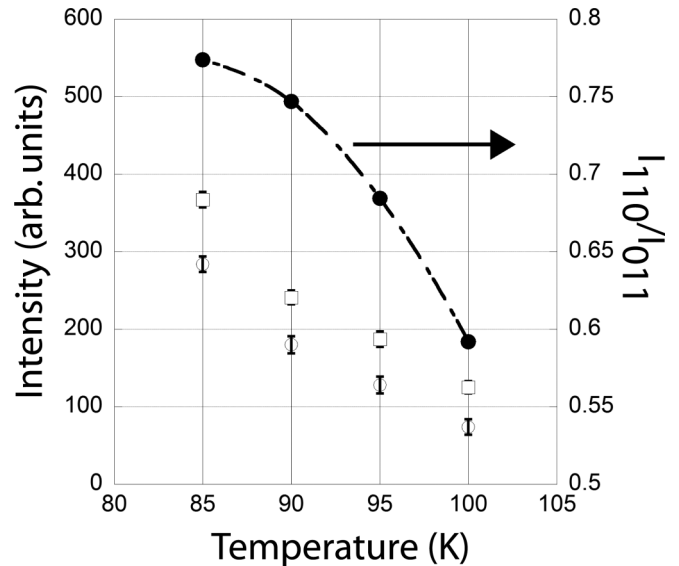


FIG. 9. Variation of the intensity of the magnetic 011 (I_{011} , open squares) and 110 (I_{110} , open circles) reflections and of the ratio I_{110}/I_{011} with temperature.

011 reflections change from $I_{110}/I_{011} \sim 0.78$ to $I_{110}/I_{011} \sim 0.59$ between 85 K and 100 K. The intensity ratio created through solely G_y - or solely G_x -type SO can be calculated as $I_{110}/I_{011} = 1.05$ and $I_{110}/I_{011} = 0.38$, respectively. This means that the G_y component decreases between 85 K and 100 K and should therefore be attributed to the decreasing $Pnma$ phase, while the G_x component should belong to the main $P2_1/a$ phase. As at the same time, the weak intensity of the 100 reflection forces the strongest component of the C -type SO to also be oriented along the crystallographic a direction, and this conclusion calls for the coexistence of two types of SO embracing either spatially or temporally different parts of the same $P2_1/a$ nuclear phase. This coexistence of spatially/temporally separated spin orders indicates that the $P2_1/a$ phase might see as well the coexistence of different orbitally ordered regions. Contrary to the $Pnma$ phase, which cannot house G -type OO, the $P2_1/a$ symmetry supports G -type and C -type orbital order. Figure 7 shows the refinement of the difference data set between 85 K and 110 K using the SO models of $C_x C_y 0$ and $G_x 00$ for the $P2_1/a$ phase and $0G_y 0$ for the $Pnma$ phase. The refined coefficients are $C_x = 0.82(1) \mu_B$, $C_y = 0.32(2) \mu_B$, and $G_x = 0.45(2) \mu_B$ for the $P2_1/a$ phase, and $G_x = 1.25(4) \mu_B$ for the $Pnma$ phase. Assuming equal moment values for the two types of SO within the $P2_1/a$ phase, this leads to a 78%/22% phase distribution for the C -type/ G -type spin orders, with each having a total moment of $\mu_V^{3+} = 0.99(2) \mu_B$. This can be compared to the results of Reehuis *et al.* [25], who determined for the monoclinic phase of YVO_3 , using the model of a single $C_x G_y C_z$ SO, very similar components for the C -type and G -type components, resulting in $\mu_V^{3+} = 1.02 \mu_B$. The solution proposed for the phase coexistence region seems at first sight complicated but has the advantage of fulfilling important criteria: The moment size and the direction of the G -type coupling ($0G_y 0$) of the $Pnma$ phase are identical to the situation at lower temperatures, where this phase is the sole nuclear phase. The $C_x C_y 0$ and the

TABLE III. IRs and their BVs of Tm situated on the Wyckoff site $4c$ for $\mathbf{k} = 0$ in space group $Pnma$.

Tm	IR1	IR2		IR3		IR4	IR5	IR6		IR7		IR8
	BV1	BV1	BV2	BV1	BV2	BV1	BV1	BV1	BV2	BV1	BV2	BV1
$x, 1/4, z$	0 1 0	1 0 0	0 0 1	1 0 0	0 0 1	0 1 0	0 1 0	1 0 0	0 0 1	1 0 0	0 0 1	0 1 0
$-x+1/2, 3/4, z+1/2$	0 -1 0	-1 0 0	0 0 1	-1 0 0	0 0 1	0 -1 0	0 1 0	1 0 0	0 0 -1	1 0 0	0 0 -1	0 1 0
$-x, 3/4, -z$	0 1 0	-1 0 0	0 0 -1	1 0 0	0 0 1	0 -1 0	0 1 0	-1 0 0	0 0 -1	1 0 0	0 0 1	0 -1 0
$x+1/2, 1/4, -z+1/2$	0 -1 0	1 0 0	0 0 -1	-1 0 0	0 0 1	0 1 0	0 1 0	-1 0 0	0 0 1	1 0 0	0 0 -1	0 -1 0
	$-C_y-$	A_x--	$--G_z$	C_x-F_z		$-A_y-$	$-F_y-$	G_x-A_z		F_x-C_z		$-G_y-$

G_x OO SO couplings within the $P2_1/a$ phase are allowed by magnetic symmetry, and the magnetic moment size adopts a value typical for the monoclinic phase region. Possible reasons for the reduced magnetic moment value of V^{3+} ($S = 1$) within the G -type OO phase were discussed by Tsvetkov *et al.* [22]. A coexistence of short-range correlations of C -type orbital order with G -type orbital order within the same nuclear phase has already been proposed earlier in the literature for YVO_3 [40]. Although allowed from symmetry considerations (Table II [26]) there is no sign of a ferromagnetic component in any of the coexisting magnetic phases.

In a very recent paper, Skoulatos *et al.* [41] proposed for $LuVO_3$ —which also adopts a monoclinic phase having C - and G -type SO components in an intermediate-temperature range—a superposition of both coupling schemes onto the V sublattice fixed in time. For $LuVO_3$, Skoulatos *et al.* found the modes $(C_x C_y 0)$ and $(G_x G_y 0)$, which are very similar to the ones found here for $TmVO_3$. In the general case, a superposition of these two modes has to lead to unequal moment values for the V sites in the sublattice. However, as in [41] $C_x \approx C_y$ and $G_x \approx -G_y$, the superposition leads to moment sizes equal within the error bars. This physical picture of the coexistence of spin orders by superimposing interference within the same crystallographic phase is less probable in the case of $TmVO_3$, because here $C_x \gg C_y$ and $G_x \gg G_y = 0$, which would lead to largely different magnetic moment values of $1.3 \mu_B$ and $0.5 \mu_B$ for crystallographically identical V sites.

For $HoVO_3$, Blake *et al.* [42] discussed the possibility of having a competition between the Jahn-Teller coupling, leading to the distortion below T_{OO} , and orbital fluctuations, which would lead to a further reduction in symmetry and, *in extremis*, to the formation of a dimerized state. The single crystal neutron data presented in [42] showed that there are significant orbital fluctuations present, which perturb the G -type OO and lead to an average structure of $HoVO_3$ better described in space group $Pb11$. We cannot exclude this possibility to exist as well for $TmVO_3$; however, our powder data, having less sensitivity than the single-crystal data of [42], do not give any indication for a further symmetry reduction of $TmVO_3$ from $P2_1/a$ below T_{OO} .

It has been shown above that the coexistence of the two OO phases is limited to the temperature region $T_S < T < T_{N1}$. Above T_{N1} and up to T_{OO} , only the G -type OO phase exists. For $SmVO_3$ [29], which is a typical example of an RVO_3 compound with an intermediate size R , a similar phase coexistence has been shown also to be restricted to the region below T_N . This means that the appearance of the C -type OO phase (having a magnetic G -type coupling) below T_N is

triggered by the appearance of the magnetic order, although the main phase with G -type OO adopts a different magnetic coupling scheme. Similar to the situation in $SmVO_3$ [29], a strong influence of the majority G -type OO phase on the minority C -type OO phase—probably through strain—can be detected within the phase coexistence region when looking at the respective unit cell volumes. At 85 K, where the phase fraction of the C -type OO phase represents about 14%, this difference amounts to only 0.07%, whereas the relaxed C -type OO phase at 50 K has a volume that is 0.15% smaller than that of the G -type OO phase (at 85 K). This value is similar to the one found for YVO_3 [19], where the transition to the C -type OO phase at lowest temperatures is also fully achieved.

C. Magnetic order of the Tm sublattice spin flop transition

Below $T_{N2} \approx 20$ K, strong changes in the intensities of the magnetic reflections are visible (Fig. 6) as the Tm sublattice becomes magnetically long-range ordered following the same magnetic propagation vector. Table III lists the allowed IRs and their BVs for the Wyckoff position $4c$ for $\mathbf{k} = 0$ using the standard notation $Pnma$ for the orthorhombic phase. At 2 K, a simple C_y -type SO corresponding to the allowed IR1 is found for the Tm site with $\mu_{Tm}^{3+} = 2.15(2)\mu_B$. Contrary to the situation found at 50 K ($0G_y 0$), the spins of the V sublattice are no longer pointing in the direction of the long b axis but follow

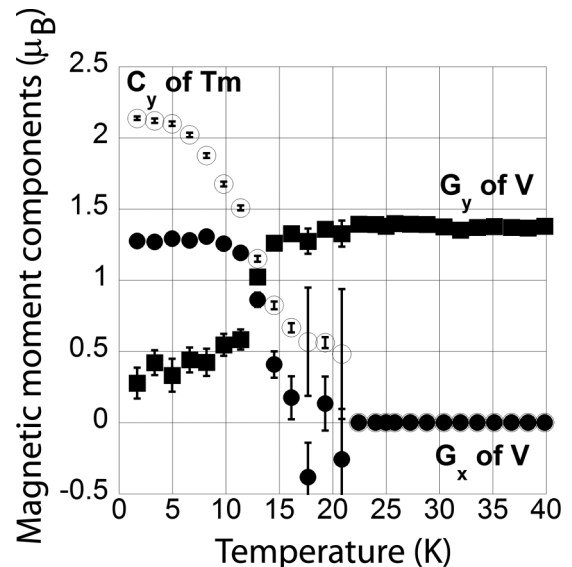


FIG. 10. Variation of the individual spin components of Tm and V with temperature.

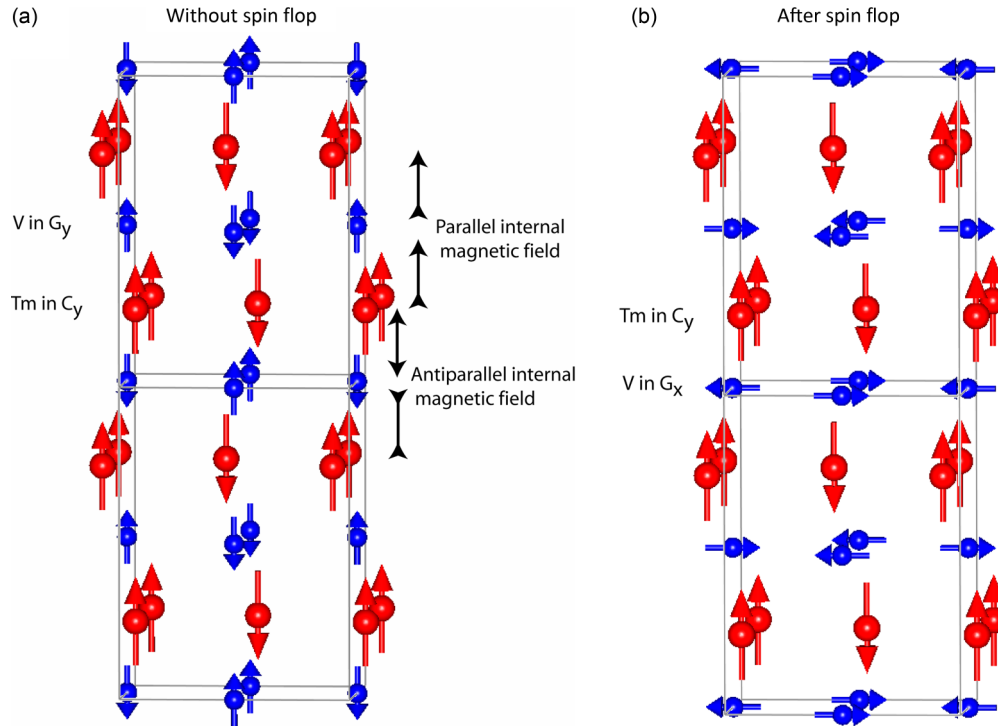


FIG. 11. (a) Sketch of a hypothetical magnetic order where the spins of the Tm^{3+} ions follow a C_y configuration and those of the V^{3+} ions follow a G_y configuration. (b) Actual magnetic structure of TmVO_3 at 2 K after a spin flop of the V spins.

a G_x00 SO. Figure 10 shows the results of a cyclic refinement of the magnetic structure between base temperature and 70 K using high intensity data.

Coming from base temperature, the spin reorientation of the V^{3+} spins is synchronized with the decline of the magnetic moment value of the Tm sublattice; at about 13 K, $G_y > G_x$. This change of SO corresponds to a spin flop transition and can be directly explained by the strong internal field created by the Tm sublattice acting on the V^{3+} sites. Figure 11(a) shows the situation where the C_y coupling of the Tm sublattice along the b direction creates a parallel internal field for one half of the V spins and an antiparallel internal field for the other half. The V subsystem reacts with a spin flop to a direction perpendicular to the internal field [Fig. 11(b)]. There is again no sign of a ferromagnetic component on the V sublattice, neither above nor below T_{N2} .

This spin flop is accompanied by a visible magnetostriction effect, leading to a decrease of the a and an increase of the c lattice parameters at $T \approx 13$ K [Figs. 3(a), 3(c)]. The other $R\text{VO}_3$ compounds with $r_{\text{R}}^{3+} \leq r_{\text{Dy}}^{3+}$ where information on the magnetic structure at base temperature is known are YVO_3 , HoVO_3 , and ErVO_3 [24,32], which all see a $0G_y0$ SO of the V spins identical to TmVO_3 above T_{N2} . The main component of the SO of the Ho sublattice in HoVO_3 is C_x , perpendicular to the G_y SO of the vanadium sublattice, and therefore not perturbing it by its strong internal field. For ErVO_3 , one has to ask oneself, however, why the strongly polarizing ordered Er sublattice, which adopts the same $0C_y0$ configuration as the Tm sublattice in TmVO_3 , does not as well lead to a spin flop transition in ErVO_3 . One reason might be that due to the low value of $T_{N2} = 2.5$ K, the spin flop has not yet taken place at the

measuring temperature of 1.6 K (value given in Table II of [31], but see [43]), or that the spin flop is hindered by a stiff lattice. In this context, it is interesting to see that the de Gennes scaling for the magnetic transition temperature of the R sublattice—which should be proportional to $(g_J - 1)^2 J(J + 1)$, where g_J is the Landé factor, and J is the total angular momentum—is not followed by ErVO_3 , which should have a T_{N2} higher than TmVO_3 .

IV. CONCLUSIONS

The neutron and synchrotron diffraction study of the temperature dependence of TmVO_3 confirms the existence of a multitude of structural and magnetic phase transitions:

(1) On cooling, a first structural transition from $Pnma$ to $P2_1/a$ takes place at $T_{O0} = 180$ K and leads to the creation of two long and two short V-O bonds symptomatic for a G -type orbital ordered phase. The monoclinic angle is small ($\gamma = 90.012^\circ$ at 110 K).

(2) At $T_{N1} = 105$ K, the magnetic order of the V sublattice induces a structural phase coexistence of a majority $P2_1/a$ and a minority $Pnma$ phase. The $P2_1/a$ phase sees a further phase separation into a volume fraction adopting a $C_x C_y 0$ magnetic coupling and a second fraction having a $G_x 00$ magnetic coupling. The $Pnma$ phase fraction orders magnetically with a $0G_y 0$ structure. At 85 K, the magnetic moment values amount to about $\mu_V = 1.0 \mu_B$.

(3) At $T_S = 75$ K, the $Pnma$ phase becomes the sole nuclear phase. Reaching a maximum value close to T_S within the $P2_1/a$ phase, the octahedral tilting is partly relieved when going through the transition to $Pnma$. This structural phase transition is accompanied by a volume contraction and the

establishment of C -type orbital order, where the V sublattice follows a $0G_y0$ magnetic coupling with $\mu_V = 1.3 \mu_B$ at 50 K.

(4) At $T_{N2} = 20$ K, the Tm sublattice orders in a C_y -type magnetic structure ($\mu_{Tm} = 2.15 \mu_B$ at 2 K) and induces a spin flop of the V sublattice from $0G_y0$ to G_x00 .

Most of these results place $TmVO_3$ into close correspondence with YVO_3 [25], which is the only other RVO_3 compound with $r_R^{3+} < r_{Dy}^{3+}$ for which detailed structural and magnetic studies have been presented. The phase coexistence of $Pnma$ and $P2_1/a$ found below T_{N1} places $TmVO_3$ at the same time in close relation to the RVO_3 compounds with $R = Sm, Eu, Gd,$ and Tb , for which a similar phase coexistence was found. $TmVO_3$ is, however, unique because the structural phase coexistence is not present down to lowest temperatures, but only between T_{N1} and T_S . The coexistence of two magnetic couplings within the C -type orbitally ordered phase with $P2_1/a$ symmetry is shared by $TmVO_3$ and $LuVO_3$. Whether the two magnetic couplings are spatially separated or superposed on the same magnetic sites remains a matter of debate. In the case of $TmVO_3$, a scenario where the two magnetic orders are present in volume fractions separated in space has been shown to be more likely. The existence of a spin flop transition of the V sublattice induced by the magnetic order of the R sublattice has not been detected before but can be explained by the strong internal field acting on the transition metal sites.

The magnetization results presented in [32] and their similitude to those of YVO_3 [11] can now be related to the phase transitions at T_{N2} , T_S , and T_{N1} found in the diffraction results. The discussion of the magnetization reversals found at T_{N1} and at T_S for YVO_3 by Ren *et al.* [16] can be equally applied to the case of $TmVO_3$. The fact that neutron diffraction did not find any sign of a ferromagnetic component, either for the $P2_1/a$ phase or for the $Pnma$ phase in $TmVO_3$ (similar to YVO_3 [25]), can be explained by the inability of neutron powder diffraction to detect magnetic moments below about $0.1 \mu_B$. The magnetization data measured under a field of 0.5 T (Fig. 3 of [32]) show strong changes in

the magnetization curves and the appearance of significant ferromagnetic components that are induced by the application of the magnetic field. A similar conclusion might be drawn as far as the existence of first-order transitions is concerned: While the zero-field neutron diffraction data did not reveal any significant thermal hysteresis, either at T_S or at T_{N1} , the magnetization data under a field of 0.5 T (Fig. 3 of [32]) showed clear signs of hysteretic behavior at T_S and T_{N1} , with widths of the hysteresis loops of about 9 K. It can be suggested that under a magnetic field, the magnetic coupling of the $Pnma$ phase sees an induced ferromagnetic component below T_S and becomes type $0G_yF_z$ (see [26]). Because the main phase fraction of the $P2_1/a$ phase above T_S has a C_xC_y0 magnetic coupling, which does not allow a ferromagnetic component (see Table II), the $Pnma$ phase should be stabilized by the magnetic field compared to the $P2_1/a$ phase and lead to the thermal hysteresis between field-cooled warming (FCW) and field-cooled cooling (FCC) curves at T_S . A similar argument should hold at T_{N1} , where the still present fraction of the $Pnma$ phase, with its induced ferromagnetic component, shifts T_{N1} to higher values on warming.

In summary, high angular resolution and high intensity neutron diffraction and synchrotron diffraction data revealed the presence of four transitions at T_{OO} , T_{N1} , T_S , and T_{N2} , which place $TmVO_3$ within the phase diagram of RVO_3 compounds corresponding to its R^{3+} ionic radius close to YVO_3 . Details like the presence of structural and magnetic phase coexistences can be found as well in RVO_3 compounds with similar R^{3+} radii; however, their temperature dependence as well as the presence of a spin flop transition are for the moment unique.

ACKNOWLEDGMENTS

Financial support from the Swedish Research Council (VR), the Göran Gustafsson Foundation, the Swedish Foundation for International Cooperation in Research and Higher Education (STINT), and the Russian Foundation for Basic Research is gratefully acknowledged.

-
- [1] J. van den Brink, G. Khaliullin, and D. Khomskii, *Phys. Rev. Lett.* **83**, 5118 (1999).
- [2] J. M. De Teresa, M. R. Ibarra, P. A. Algarabel, C. Ritter, C. Marquina, J. Blasco, J. Garcia, A. del Moral, and Z. Arnold, *Nature* **386**, 256 (1997).
- [3] N. Aliouane, O. Prokhnenko, R. Feyerherm, M. Mostovoy, J. Stempffer, K. Habicht, K. C. Rule, E. Dudzik, A. U. B. Wolter, A. Maljuk, and D. N. Argyriou, *J. Phys.: Condens. Matter* **20**, 434215 (2008).
- [4] G. Sankar, J. M. Thomas, V. Varma, G. U. Kulkarni, and C. N. R. Rao, *Chem. Phys. Lett.* **251**, 79 (1996).
- [5] A. Maignan, C. Martin, D. Pelloquin, N. Nguyen, and B. Raveau, *J. Solid State Chem.* **142**, 247 (1999).
- [6] F. Fauth, E. Suard, V. Caignaert, and I. Mirebeau, *Phys. Rev. B* **66**, 184421 (2002).
- [7] J. B. Torrance, P. Lacorre, A. I. Nazzal, E. J. Ansaldo, and C. Niedermayer, *Phys. Rev. B* **45**, 8209 (1992).
- [8] D. D. Sarma, N. Shanthi, and P. Mahadevan, *J. Phys. Condens. Matter* **6**, 10467 (1994).
- [9] M. Medarde, *J. Phys. Condens. Matter* **9**, 1679 (1997).
- [10] N. Shirakawa and M. Ishikawa, *Jpn. J. Appl. Phys.* **30**, L755 (1991).
- [11] Y. Ren, T. T. M. Palstra, D. I. Khomskii, E. Pellegrin, A. A. Nugroho, A. A. Menovsky, and G. A. Sawatzky, *Nature* **396**, 441 (1998).
- [12] M. J. Martinez-Lope, J. A. Alonso, M. Retuerto, and M. T. Fernandez-Diaz, *Inorg. Chem.* **47**, 2634 (2008).
- [13] A. S. Borukhovich, G. V. Bazuev, and G. P. Shveikin, *Sov. Phys. Solid State* **16**, 191 (1974).
- [14] V. G. Zubkov, G. V. Bazuev, and G. P. Shveikin, *Sov. Phys. Solid State* **18**, 1165 (1976).
- [15] H. Kawano, H. Yoshizawa, and Y. Ueda, *J. Phys. Soc. Jpn.* **63**, 2857 (1994).
- [16] Y. Ren, T. T. M. Palstra, D. I. Khomskii, A. A. Nugroho, A. A. Menovsky, and G. A. Sawatzky, *Phys. Rev. B* **62**, 6577 (2000).
- [17] H. Sawada, N. Hamada, K. Terakura, and T. Asada, *Phys. Rev. B* **53**, 12742 (1996).

- [18] T. Mizokawa and A. Fujimori, *Phys. Rev. B* **54**, 5368 (1996).
- [19] G. R. Blake, T. T. M. Palstra, Y. Ren, A. A. Nugroho, and A. A. Menovsky, *Phys. Rev. B* **65**, 174112 (2002).
- [20] P. Bordet, C. Chailout, M. Marezio, Q. Huang, A. Santoro, S.-W. Cheong, H. Takagi, C. S. Oglesby, and B. Batlogg, *J. Solid State Chem.* **106**, 253 (1993).
- [21] C. Ulrich, G. Khaliullin, J. Sirker, M. Reehuis, M. Ohl, S. Miyasaka, Y. Tokura, and B. Keimer, *Phys. Rev. Lett.* **91**, 257202 (2003).
- [22] A. A. Tsvetkov, F. P. Mena, P. H. M. van Loosdrecht, D. van der Marel, Y. Ren, A. A. Nugroho, A. A. Menovsky, I. S. Elfimov, and G. A. Sawatzky, *Phys. Rev. B* **69**, 075110 (2004).
- [23] S. Miyasaka, Y. Okimoto, M. Iwama, and Y. Tokura, *Phys. Rev. B* **68**, 100406(R) (2003).
- [24] M. Reehuis, C. Ulrich, P. Pattison, M. Miyasaka, Y. Tokura, and B. Keimer, *Eur. Phys. J. B* **64**, 27 (2008).
- [25] M. Reehuis, C. Ulrich, P. Pattison, B. Ouladdiaf, M. C. Rheinstädter, M. Ohl, L. P. Regnault, M. Miyasaka, Y. Tokura, and B. Keimer, *Phys. Rev. B* **73**, 094440 (2006).
- [26] Magnetic symmetry analysis gives the allowed IRs $G_x C_y A_z$, $C_x G_y F_z$, $A_x F_y G_z$, and $F_x A_y C_z$ for Wyckoff site $4b$ in space group $Pnma$ and $\mathbf{k} = 0$.
- [27] G. R. Blake, T. T. M. Palstra, Y. Ren, A. A. Nugroho, and A. A. Menovsky, *Phys. Rev. Lett.* **87**, 245501 (2001).
- [28] M. H. Sage, G. R. Blake, C. Marquina, and T. T. M. Palstra, *Phys. Rev. B* **76**, 195102 (2007).
- [29] M. H. Sage, G. R. Blake, G. J. Nieuwenhuys, and T. T. M. Palstra, *Phys. Rev. Lett.* **96**, 036401 (2006).
- [30] A. Munoz, J. A. Alonso, M. T. Casais, M. J. Martinez-Lope, J. L. Martinez, and M. T. Fernandez-Diaz, *J. Mater. Chem.* **13**, 1234 (2003).
- [31] M. Reehuis, C. Ulrich, K. Prokes, S. Mat'as, J. Fujioka, S. Miyasaka, Y. Tokura, and B. Keimer, *Phys. Rev. B* **83**, 064404 (2011).
- [32] T. Sarkar, S. A. Ivanov, G. V. Bazuev, P. Nordblad, and R. Mathieu, *J. Phys. D: Appl. Phys.* **48**, 345003 (2015).
- [33] T. C. Hansen, P. F. Henry, H. E. Fischer, J. Torregrossa, and P. Convert, *Meas. Sci. Technol.* **19**, 034001 (2008).
- [34] F. Fauth, I. Peral, C. Popescu, and M. Knapp, *Powder Diffraction* **28**, S360 (2013).
- [35] J. Rodriguez-Carvajal, *Physica B* **192**, 55 (1993).
- [36] J. Rodriguez-Carvajal, BASIREPS: a program for calculating irreducible representations of space groups and basis functions for axial and polar vector properties. Part of the FullProf Suite of programs, www.ill.eu/sites/fullprof/.
- [37] C. Ritter, *Solid State Phenom.* **170**, 263 (2011).
- [38] J. B. Goodenough, *Prog. Solid State Chem.* **5**, 145 (1971).
- [39] T. Mizokawa, D. I. Khomskii, and G. A. Sawatzky, *Phys. Rev. B* **60**, 7309 (1999).
- [40] S. Miyasaka, J. Fujioka, M. Iwama, Y. Okimoto, and Y. Tokura, *Phys. Rev. B* **73**, 224436 (2006).
- [41] M. Skoulatos, S. Toth, B. Roessli, M. Enderle, K. Habicht, D. Sheptyakov, A. Cervellino, P. G. Freeman, M. Reehuis, A. Stunault, G. J. McIntyre, L. D. Tung, C. Marjerrison, E. Pomjakushina, P. J. Brown, D. I. Khomskii, Ch. Rüegg, A. Kreyssig, A. I. Goldman, and J. P. Goff, *Phys. Rev. B* **91**, 161104(R) (2015).
- [42] G. R. Blake, A. A. Nugroho, M. J. Gutmann, and T. T. M. Palstra, *Phys. Rev. B* **79**, 045101 (2009).
- [43] Looking at fig. 2 of [31], it seems that the magnetic reflections used to determine the SO of the vanadium sublattice in ErVO_3 have not been measured below 6 K, which would explain the fact that a spin flop has not been seen in this compound.